Proceedings of the 9th International Conference on Structural Dynamics, EURODYN 2014
Porto, Portugal, 30 June - 2 July 2014
A. Cunha, E. Caetano, P. Ribeiro, G. Müller (eds.)
ISSN: 2311-9020; ISBN: 978-972-752-165-4

Reliability of high-speed railway bridges with respect to uncertain characteristics

Patrick Salcher[1], Helmuth Pradlwarter[1], Christoph Adam[1]
[1]Unit of Applied Mechanics, University of Innsbruck, Technikerstr. 13, 6020 Innsbruck, Austria
email: Patrick.Salcher@uibk.ac.at, Helmut.Pradlwarter@uibk.ac.at, Christoph.Adam@uibk.ac.at

ABSTRACT: The prediction of the dynamic response of railway bridges subjected to high-speed trains is investigated by stochastic methods to account for the unavoidable uncertainties. In this contribution Latin hypercube and line sampling is used for Monte Carlo simulations on a simple beam bridge model, to provide an overall overview of the structural reliability considering frequency variation, uncertain damping, and structural parameters. In particular, acceleration amplitudes define the limit states of the bridge models. Frequency uncertainties are a result of temperature induced stiffness changes and varying maintenance states of the bridge structure. With variation of the natural frequencies and bridge damping, both resonance speeds and the magnitudes of the resonance peaks are uncertain. Alternatively, on a more elaborated finite element bridge model, the influence of these uncertainties is investigated. The outcomes of the stochastic mechanical models with different degree of sophistication are compared with results of deterministic computations according to design guidelines.

KEY WORDS: Dynamic response; Environmental impact; High-speed train; Line sampling; Railway bridge; Reliability

1 INTRODUCTION

More recently, the demand on reliable dynamic response prediction for bridges has been increased with the development of new high-speed railway lines. Excessive vibrations of these bridges may cause several problems, such as ballast instability and derailment due to loss of wheel-rail contact, and fatigue problems within the structure may arise. Additionally to passenger safety also passenger comfort must be ensured when a train passes a bridge. Consequently, several design guidelines [1-3] have been established to avoid these problems. These guidelines recommend creating a computational model that reproduces a kind of worst-case response scenario. This conservative approach is, however, non-economical, and furthermore, in many cases an unambiguous model cannot be defined when some of the relations that influence the dynamic response significantly are unknown. Some of the mentioned problems may even occur, although the design rules are satisfied. This may be the case for travelling speeds slightly below the maximum speed for which, according to guidelines, a quasi-static approach is sufficient.

The dynamic response prediction of railway bridges is usually based on a deterministic approach, both in the design process and in research, although many uncertainties in the model parameters are present. The natural frequencies of the structure, for example, can vary with the temperature or with nonlinear response amplitudes. Furthermore, the real energy dissipation mechanism is quite complex. Nevertheless, commonly simple mechanical models of bridge damping are used, with parameters chosen by experience. By treating these uncertainties as random variables with a specific distribution its possible to compute estimates of the probability of bridge failure due to defined limit states. In the following, this stochastic approach is applied when analyzing two example bridges using mechanical models of different degree of sophistication.

2 NUMERICAL MODELS

In this contribution, high-speed train passing through a bridge is modeled as a sequence of moving single forces of constant speed v. Thus, the positive effect of vehicle bridge interaction is only considered by assigning additional damping to the bridge model. For examining the general response behavior of a railway bridge, simply supported single span structures with a single track are analyzed.

2.1 Simple bridge model

In the simpler approach it is assumed that the response of the bridge including rails, sleepers, ballast and supporting structure, is described sufficiently accurate by a *Bernoulli-Euler* beam (see Figure 1 a) with constant structural parameters (mass per unit length ρA, bending stiffness EI). Without damping the equation of motion for the vertical deflection $w(x,t)$ of this problem reads as [4, 5]:

$$\rho A\ddot{w} + EIw_{xxxx} = \sum_i F_i \delta(x-\xi_i)\mathrm{X}_i(t) \tag{1}$$

$$\mathrm{X}_i(t) = \left[H(t-t_{i,0}) - H(t-t_{i,E}) \right] \tag{2}$$

Herein, the ith axial force F_i of the train is multiplied by the Dirac delta function δ evaluated at the actual position $\xi_i = vt - s_i$ of the force on the beam and a window function $\mathrm{X}_i(t)$ composed of two Heaviside functions H, with the initial position s_i and the travel speed v of the force. The window function serves as a switch, when F_i enters ($t = t_{i,0}$) and leaves the beam ($t = t_{i,E}$). Applying modal analysis and taking into account M mode shapes $\phi_n(x)$ ($n = 1, 2, .., M$), the beam deflection is expressed as $w(x,t) = \sum_{n=1}^{M} \phi_n(x) q_n(t)$,

yielding M decoupled ordinary oscillator equations for the modal coordinates $q_n(t)$,

$$\ddot{q}_n + 2\zeta_n\omega_n\dot{q}_n + \omega_n^2 q_n = \frac{1}{m_n}\sum_i F_i\phi_n(\xi_i)\mathrm{X}_i \qquad (3)$$

where damping ζ_n has been added modally. With the circular natural frequencies ω_n and modal masses m_n ($n=1,...,M$) of the actual beam problem the computation of the deflection $w(x,t)$ and the acceleration $\ddot{w}(x,t)$ is straightforward. In the present study five modes approximate the modal series, with all modal damping factors equal, i.e. $\zeta_n = \zeta$.

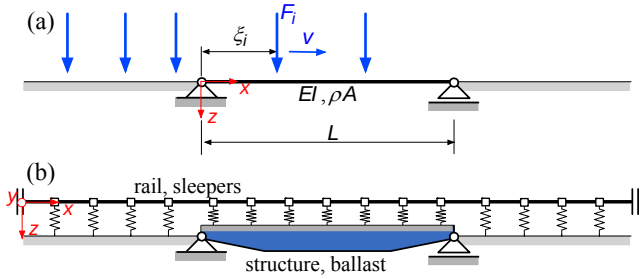

Figure 1. Mechanical bridge models: (a) *Bernoulli-Euler* beam bridge and (b) elaborated 3D-FE bridge (side view).

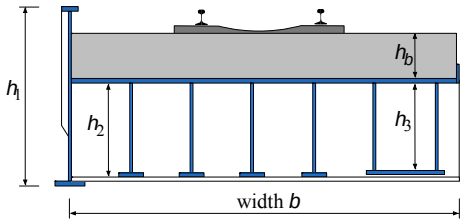

Figure 2. Cross-section of the elaborated 3D-FE bridge.

2.2 *Elaborated bridge model*

An elaborated three-dimensional (3D) finite element (FE) model is used as a more realistic example of a railway bridge (see Figure 1 b and Figure 2). The supporting structure is discretized with beam and shell elements, considering the additional mass of the ballast bed. Point mass elements characterize the effect of the sleepers, and they are connected via springs to the structure to take into account the ballast stiffness. *Bernoulli-Euler* beam elements model the rails. A substructure approach as proposed in [4] based on modal analysis is used to compute the nodal deflections $\mathbf{u}_{FE}(t)$ and the nodal accelerations $\ddot{\mathbf{u}}_{FE}(t)$ of the bridge. Viscous damping is considered modally, with each damping ratio assumed to be equal, i.e. $\zeta_n = \zeta$.

2.3 *High-speed train load set*

For designing high-speed railway bridges according to European standards and provisions such as Eurocode 1 (EC1) [2] the load pattern generated by the moving single forces must be adjusted to static axle loads and axle spacing of the expected local train traffic. In addition, a high-speed load model (HSLM) consisting of a set of universal trains must be considered to ensure the interoperability of existing trains. Note that future rolling stock must be designed according to the HSLM train set to make sure that existing bridges can be crossed safely. Consequently, in this paper the considered bridge models are subjected to the HSLM-A train set to compare the derived estimates of the structural safety with the semi-probabilistic approach of EC1 [2]. This set consists of ten individual trains with different numbers of wagons, different axle spacing and axle loads, as specified in [2].

3 UNCERTAINTIES

3.1 *Damping*

One of the most important sources of uncertainty in the mechanical model is inherent structural damping. Energy dissipation is a result of various mechanisms within the structure. Friction in the joints, ballast and supports, hysteresis damping of the structural components, and the aerodynamic resistance of the bridge are sources of damping. Nevertheless the rather simply model of viscous damping, generally used in structural engineering problems, is applied to account for all energy dissipation effects.

Clearly, the magnitude of the damping coefficient ζ varies in a wide range depending on the bridge type and structure. Although damping can be measured after completion of the bridge, an estimate is already required in the design process. Especially in a state of resonance, damping has a distinct influence on the dynamic peak response of the bridge. In Fryba [6] the damping coefficient ζ (expressed as the logarithmic damping decrement ϑ) is documented for different types of railway bridges. Figure 3 shows these damping coefficients for steel bridges and their mean values (black line) with respect to the bridge span. The blue line represents the damping coefficient for steel bridges according to EC1, taking into account increased damping for span length smaller than 20 m, i.e. $L < 20$ m. It is readily observed that this line is a lower bound of the data revealed from measurements. In many cases this approach leads to conservative response predictions, and is therefor uneconomical. The red line represents the maximum damping coefficient according to the EC1 that accounts for bridge-vehicle interaction (BVI) effects in bridges with spans $L < 30$ m.

For the stochastic bridge models used in this study, the modal damping coefficient ζ is assumed to be a lognormally distributed random variable with all random quantities positive. To exclude very unlikely low damping values a lognormal distribution with a cut-off is subject of further research.

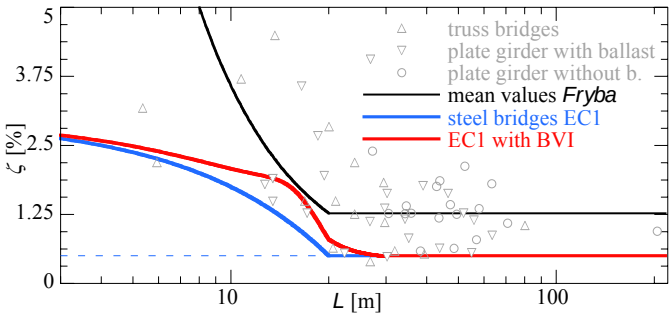

Figure 3. Modal damping coefficients ζ for steel bridges according to [2] and [6].

3.2 *Environmental influences*

Changes of the environmental conditions may modify the dynamic behavior of the structure. For instance, in many bridges the stiffness, and in further consequence the natural frequencies, increase considerably when the temperature T drops below the freezing point due to frozen water within the ballast and the ground [7]. Several measurement campaigns on real bridges (e.g. [7-10]) have revealed that this stiffness modification results in more or less bilinear temperature-natural frequency relationship. Thus, in the present study a bilinear function of the fundamental natural frequency f_1 with respect to the temperature T as shown in Figure 4 is assumed. The temperature is modeled as a random variable according to an extreme value distribution. In the numerical simulations based on the simple *Bernoulli-Euler* beam model the bending stiffness EI is modified to obtain the fundamental natural frequency according to the relationship defined in Figure 4.

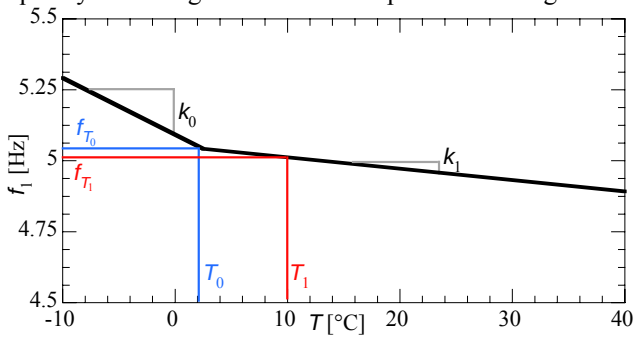

Figure 4. Bilinear relationship between the fundamental natural frequency and the environmental temperature.

Adopting of this black box-like treatment of the temperature-frequency relation to the more detailed finite element model is not straightforward. In a preliminary approach, here the ballast density δ^b and ballast stiffness $k^b_{x,y,z}$ is treated as random variable to account for the environmental impact on the bridge. Similar to the approach used in [11] a uniform distribution describes the density with limits specified in [3] and [12]. For the ballast stiffness a normal distribution with a mean according to [3] and a coefficient of variance CV = 0.1 is chosen. Table 1 provides the random variables for this bridge model. Note that a more realistic consideration of temperature effects in the 3D-FE model requires further research.

3.3 *Other uncertainties*

For the 3D-FE bridge model also material and geometric uncertainties are considered, see Table 1. Full correlation between Young's modulus E and Poisson's ratio ν of the steel members is assumed, whereas all other variables are taken as uncorrelated. In the model the thickness of the ballast follows a uniform distribution. A geometric factor β_G accounts for inaccuracies of height and width of the flanges of the main girders. These factors are chosen with a Gaussian distribution according to the guidelines specified in [13], however selecting smaller CVs because the set-up of the investigated structure shown in Figure 2 is simple, and thus, the uncertainties are expected to be small.

4 PERFORMANCE FUNCTION

Assuming sufficient resistance for static loads, the capacity of a railway bridge must also be ensured for dynamic loads from the high-speed train passage. Note only the internal forces are limited but also several other thresholds must not be exceeded. For example, the angle of twist and the vertical deflection of the bridge deck are limited to prevent derailing.

According to [14] for vertical deck accelerations $a_{z,1}$ > 7 m/s^2 the ballast becomes instable, and therefore, the rail settlement is increased, leading to a higher maintenance frequency of the bridge. When the vertical acceleration $a_{z,2}$ exceeds 10 m/ s^2, the risk of derailing is high. Consequently, also the maximum deck acceleration, which serves in the following examples as limit state, needs to be checked. According to the design guidelines [2, 3] these acceleration limits in combination with a safety factor of 2 must be satisfied for travel speeds v larger than 55.56 m/s, to provide a negligible risk of these failure modes. EC1 [2] requires a design speed 20% larger than the conceptual maximum travel speed (i.e. $v_0 = 1.2 v_E$) when comparing the results of a stochastic computation with these deterministic design rules.

In contrast, a reliability analysis provides an estimate of the failure probability. The limit value $a_{z,1}$ is classified as a fatigue limit state, for which a failure probability $p_F < 10^{-4}$ is specified (EN1990 [1] for RC2 class buildings). For ultimate limit states with the threat of human life such as derailing, a failure probability of $p_F < 10^{-6}$ is the European standard. To evaluate the failure probabilities of a bridge subjected to the train set HSLM-A with a design speed v_0 with respect to the acceleration limit a_z, the limit state function $g(\mathbf{x}, v_0)$ for given set of random parameters $\mathbf{x} = (X_1, X_2, ..., X_n)$ is derived according to:

$$g(\mathbf{x}, v_0) = a_z - \max\left(\ddot{w}(X_1, X_2, ..., X_n, v \le v_0)\right) \qquad (4)$$

The failure state of the bridge is reached for $g(\mathbf{x}, v_0) < 0$, giving the indicator function $1_F(\mathbf{x}, v_0) = 1$. In a safe condition $g(\mathbf{x}, v_0) > 0$ and $1_F(\mathbf{x}, v_0) = 0$.

4.1 *Simulation methods*

Reliability analysis of the present study is based on Monte Carlo simulations (MC) with standard random samples and Latin hypercube samples (LH) [15-17]. Simple counting of all failed samples and dividing by the sample size N gives an estimator of probability of failure:

$$\hat{p}_F = \frac{1}{N} \sum_{i=1}^{N} 1_F(\mathbf{x}_i, v_0) \qquad (5)$$

These methods are also quite useful for visualizing the response variability in a spectral representation (see Figures 6 to 8). Although the application of LH sampling reduces the sample size significantly [15, 17], this method is still computationally expensive, especially for a more elaborated bridge model. Hence, in this study line sampling (LS) [18, 19] is adopted to estimate the probability of failure with less computational effort, as shown in Figure 5. Given that the critical acceleration response $\max \ddot{w}(\mathbf{x}, v_0)$ for R random

variables increases in the important direction defined by unit vector $\mathbf{e}^{imp}$, its kth entry is evaluated according to:

$$e_k^{imp} = s(X_k) / \sqrt{\sum_{k=1}^{R} s(X_k)^2} \tag{6}$$

Herein is $s(X_k)$ a measure of the importance of the kth random variable X_k with standard distribution σ_k [20]:

$$s(X_k) = \frac{\partial g(\mathbf{x}, v_0)}{\partial X_k} \sigma_k \tag{7}$$

The set of random variables $\mathbf{x}$ and unit vector $\mathbf{e}^{imp}$ is transformed into standard normal space, yielding a set of standard normal distributed random variables $\mathbf{u}$ and the important direction unit vector $\mathbf{e}_u^{imp}$ in the transformed space. From each representation U_n of a random sample of size N in this space, the boundary of the failure region, defined by $g(\mathbf{u}, v_0) = 0$, is found iteratively in the direction $\mathbf{e}_u^{imp}$. The probability of failure $p_F(U_n)$ along a random "line" is given by a one-dimensional normal distribution (see Figure 5). An estimator of p_F for line sampling is [18]:

$$\hat{p}_F = \frac{1}{N} \sum_{n=1}^{N} p_F(U_n) \tag{8}$$

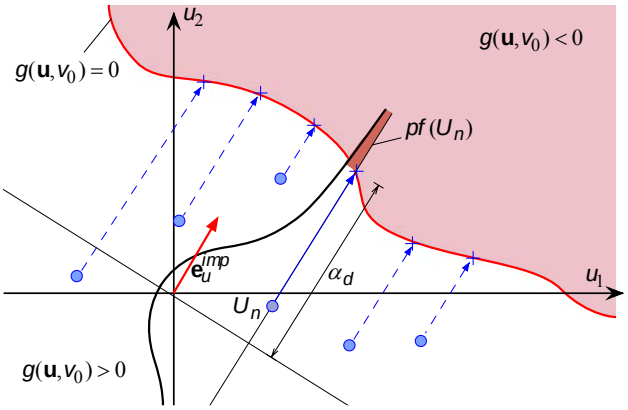

Figure 5. LS procedure in standard normal space.

5 SIMPLE BRIDGE PROBLEM

5.1 *General response behavior*

To provid a global view of the response behavior of a railway bridge with uncertain parameters, a short simply supported single span bridge is investigated, which is modeled as *Bernoulli-Euler* beam (span length: $L = 17.5$m, fundamental natural frequency at $T_1 = 10$°C: $f_{T_1} = 5.0$ Hz. The modal damping values ζ and the temperature T are modeled as uncertain random quantities with distributions specified above, and mean μ and CV according to Table 1. A bilinear temperature-frequency relationship as shown in Figure 4 is assumed to hold true, with $T_0 = 2.5$°C, and the negative slopes for both linear branches $k_0 = 0.02$ and $k_1 = 0.004$, respectively.

The scatter of the maximum acceleration response $\ddot{w}(x,t)$ induced by the 10 trains of the HSLM-A set is visualized in Figure 6. Since the maximum acceleration may occur at a travel speed v smaller than the design speed v_0, the maximum response value of the entire speed range $v < v_0$ is depicted in terms of the non-dimensional speed parameter $S_0(T) = 2v_0 / f_1(T)L$, as introduced in [5]. Each grey line corresponds to the bridge peak acceleration response excited by one train, at the mean values of the random parameters. The solid blue line envelopes the mean response of all trains, and represents the maximum acceleration for the train set with design speed v_0. A variation of the damping coefficient ζ shifts this line towards the quantiles of the maximum acceleration response that are shown with dashed blue lines, indicated with a blue arrow. The vertical solid line represents, for a given design speed v_0, the mean value of $S_0(T)$. Since a change of the temperature T changes the fundamental frequency f_1, this limit is shifted to the left if T becomes smaller (f_1 increases) and to the right if T increases (f_1 decreases), respectively, as indicated by the red arrow.

In this model the effect of both random variables on the acceleration response is decoupled. Variation of damping directly influences the maximum acceleration response at mean speed S_0, especially in a state of resonance. On the other hand, a temperature change and the corresponding frequency change only shifts the resonance peaks to different speeds v. Hence, the boundaries of S_0 are moved without affecting the response magnitude. In speed ranges where the gradient of the response envelope (blue line) is zero, the maximum acceleration is, thus, not changed. However, when another resonance peak is moved in- or outside the speed range up to S_0 it can induce a large in- or decrease of this response quantity.

Figure 7 visualizes the variability of the envelope of the maximum bridge acceleration response, plotted against the actual travel speed v. In addition to mean, 15% and 85%

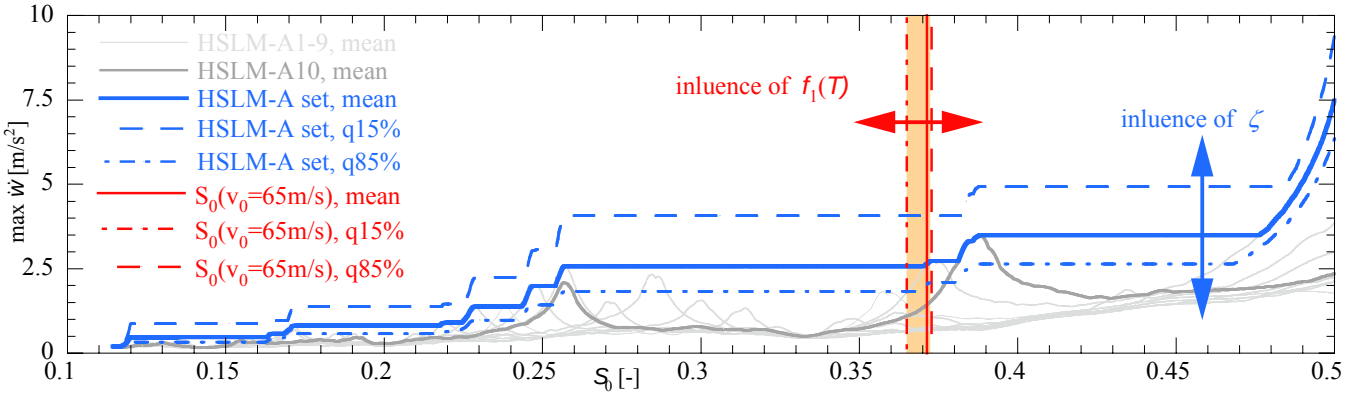

Figure 6. Uncertain maximum acceleration for uncertain natural frequency and damping.

quantiles also the minimum and maximum spectra of a standard Monte Carlo simulation with 5000 samples are plotted. Figure 8 contains the same data, however, here the maximum acceleration in the speed range $0 \le v \le v_0$ is plotted against the design speed v_0. These figures reveal that the expected maximum acceleration varies considerably, i.e. the quantiles deviate 38% from the mean.

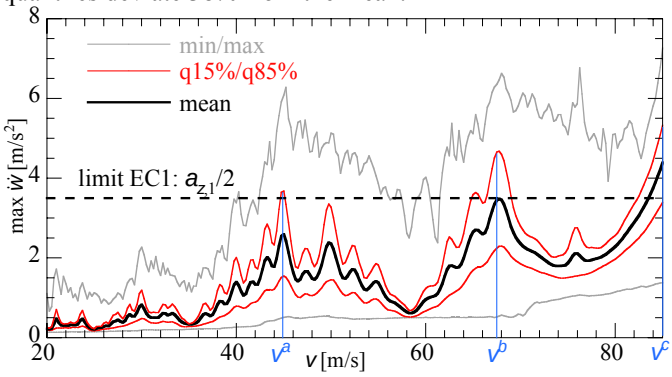

Figure 7. Spectrum of maximum acceleration of the beam bridge subjected to the HSLM-A train set with respect to the actual train speed v.

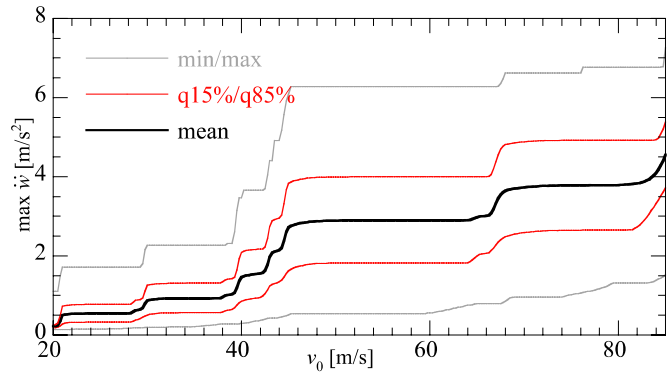

Figure 8. Spectrum of maximum acceleration of the beam bridge subjected to the HSLM-A train set with respect to the design speed v_0.

5.2 *Probability of failure*

The parameters of the bridge are tuned to yield a deterministic maximum bridge response that corresponds to the acceleration limit $a_{z,1}/2 = 3.5$ m/s^2 (according to EC1) for a design speed of $v_0 = 83.3$ m/s. For this deterministic bridge the fundamental frequency f_1 is equal to f_{T1}, and the damping coefficient ζ is the mean specified in Table 1, i.e. $\zeta = 0.01$. In Figure 7 a dashed black line represents the limit value $a_{z,1}/2 = 3.5$ m/s^2. Consequently, the deterministic bridge assessment for a safety factor of 2 can be compared with the failure probability of the proposed stochastic model. An estimator for the probability of failure $\hat{p}_F$ for different acceleration limit values a_z and a design speed of $v_0 = 85.0$ m/s is determined with the methods mentioned above.

Figure 9 reveals the advantage of LS. With increasing sample size N all methods (MC, LH and LS) converge to the same estimates of the probability of failure. For LS, a sample of $N = 100$ realizations already gives accurate results, proving its efficiency compared to the other methods. Although within the iterative procedure more points need to be evaluated, the boundary of the failure domain is usually found within two to four iterations. For higher acceleration limits a_z, Figure 9 and Figure 10 show that the probability of failure is decreasing fast, therefore large sample sizes are needed for MC and LH methods and making for this application LS the preferred method. In Figure 11, the estimate of $\hat{p}_F$ (LS, $N = 100$) is displayed for different design speeds and the threshold value of $a_{z,1} = 7.0$ m/s^2. Within the considered speed range the estimates of p_F comply with the postulated failure probability. According to this stochastic model a speed limit of $v_E = 85.0$ m/s can be approved compared to the allowed speed of $v_E = 83.3 / 1.2 = 69.4$ m/s based on the deterministic concept.

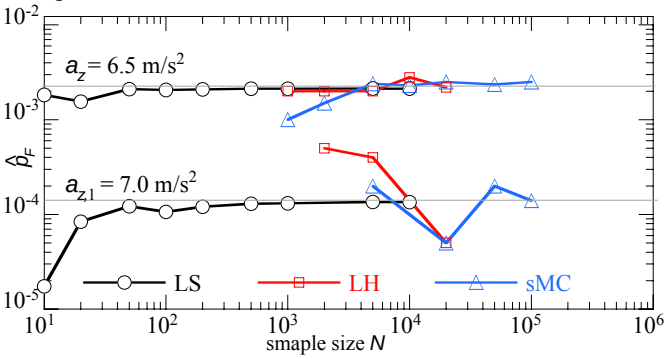

Figure 9. Estimates of the probability of failure for different simulation methods, sample sizes and limit states.

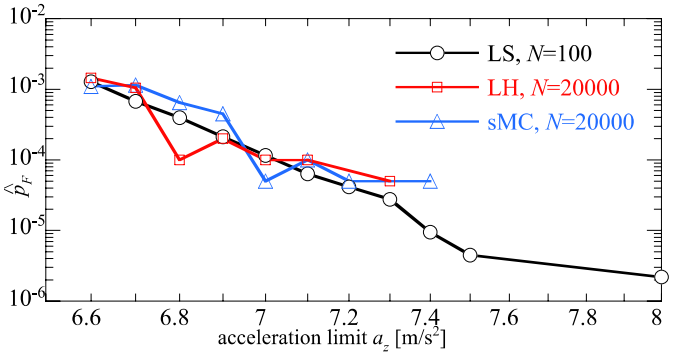

Figure 10. Estimates of the probability of failure for increasing acceleration limits.

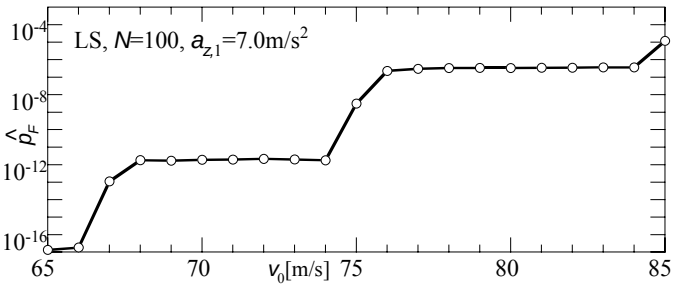

Figure 11. Estimates of the probability of failure for increasing design speed v_0.

5.3 *Effect of the temperature-frequency relation*

The resulting failure probabilities depend strongly on the model and on its uncertain variables. The large impact of the

damping parameter and its distribution has already been discussed before. Here the effect of the underlying temperature-frequency relationship (as shown in Figure 4) is studied, by varying the negative slopes k_0 and k_1. Assuming a linear behavior for $k_0 = k_1$, in Figure 12 the 15%, 50%, and 85% quantiles of the maximum acceleration (MC, $N = 5000$) for resonance speeds $v^a = 45.0$ m/s (red) and $v^b = 67.5$ m/s (blue), and speed $v^c = 85.0$ m/s (black) are plotted against the slope k_0. These particular speeds are highlighted in Figure 7. It can be seen that with increasing negative slope the median acceleration decreases slightly for v^a and v^b. In contrast, this response quantity slightly increases for v^c combined with a strong increase of the acceleration variability. This behavior is a result of the shift of the resonance peaks of the spectrum. While speeds v^a and v^b represent a resonance peak, v^c is ahead of a peak, and thus yields an increase of the acceleration and its variability.

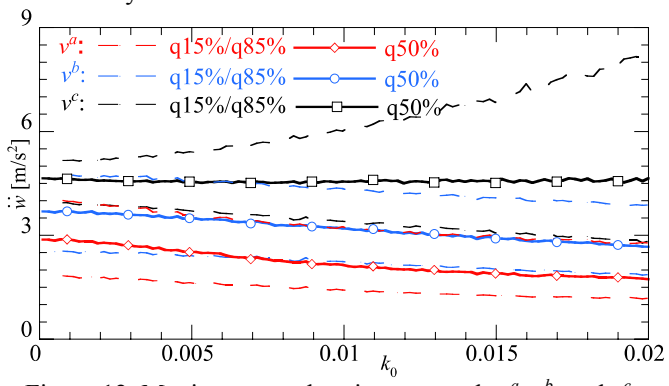

Figure 12. Maximum acceleration at speeds v^a, v^b, and v^c. Linear temperature-frequency relation, $k_1 = k_0$.

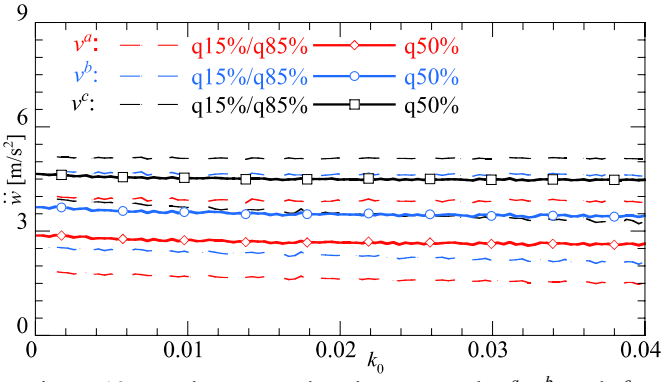

Figure 13. Maximum acceleration at speeds v^a, v^b, and v^c. Bilinear temperature-frequency relation, $k_1 = 0.001$.

Figure 13 visualizes the same response quantity for a bilinear temperature-fundamental frequency (T-f_1) relation with $k_1 = 0.001 = const$ and slope variation for freezing temperatures k_0. In this situation for all considered speeds $v^{a\text{-}c}$ a decrease of the acceleration is observed. The stiffness increase due to low temperatures shifts the resonance peaks to higher speeds, and thus, beyond the considered speed range. Figure 14 shows the probability of failure $\hat{p}_F$ for these two cases exemplarily for a design speed of $v_0 = 85.0$ m/s. For the linear temperature-frequency relation $\hat{p}_F$ rises fast, because with increasing temperatures natural frequencies become smaller. The results of this figure reveal that an increase of the natural frequency due to frost has no negative effect on the bridges acceleration response with respect to design limits (red line).

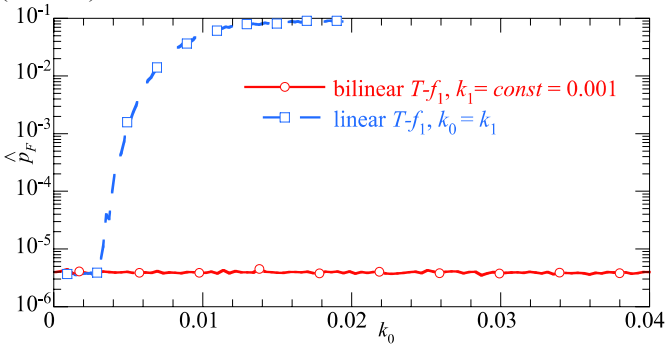

Figure 14. Probability of failure, LS $N = 100$.

6 ELABORATED BRIDGE MODEL

6.1 *Example bridge*

As a further example problem a steel bridge composed of two mirror-symmetric simply supported beam-like structures carrying the two tracks is examined. One half of the bridge structure, with a cross section as displayed in Figure 2, is modeled as 3D-FE model, considering rails, sleepers, ballast, and the supporting structure. The span L of the bridge is 16.8 m, its width b is 4.67 m, and the main girders heights [h_1, h_2, h_3] are [2.09, 1.14, 1.10] m. Ten transversal oriented I-girders distributed equally over the span provide cross stiffing. The bridge is subjected to the trains of the HSLM-A set. In the numerical simulations the first ten modes are taken into account. In the underlying deterministic bridge model with assigned mean values of the uncertain parameters, thus, all modes up to 30 Hz are included in the analysis.

Table 1. Random variables for both example bridges.

Model	Nr. (X_k)	Random variable	Distribution	μ /min (uniform)	CV /max (uniform)
Bernoulli-Euler	1	Temperature T [°C]	Extreme value	8.97	1.02
beam	2	Modal damping ζ [%]	Lognormal	1.00	0.66
	1, 6	Steel bridge/rail E [N/m^2]	Gaussian	2.1e11	0.03
	2, 7	Steel bridge/rail ν	Gaussian	0.30	0.03
	3	Ballast density δ^b [kg/m^3]	Uniform	1900.0	2000.0
3D-FE	4	Ballast height h_b [m]	Uniform	0.55	0.65
	5	Ballast stiffness factor β_k	Gaussian	1.00	0.10
	8-20	Girder geometric factor β_G	Gaussian	1.00	0.01
	21	Modal damping ζ [%]	Lognormal	1.05	0.60

6.2 *Parameter uncertainties*

A total number of 21 parameters are considered as uncertain, and they are listed in Table 1 together with distributions, mean values and coefficients of variance, or alternatively min- and max-limits in the case of uniform distributions. According to EC1 for this bridge the maximum allowed damping is $\zeta = 1.5\%$, compare with Figure 3. For the stochastic model the random variable X_{21} stands for the modal damping values $\zeta_n = \zeta$. The underlying log-normal distribution is adjusted with the result that the median of X_{21} fits the maximum damping value according due EC1 ($\zeta = 0.9\%$) without taking account BVI. The 15% and 85% quantiles correspond to damping values of $\zeta = 0.5\%$ and $\zeta = 1.6\%$, respectively.

As an outcome of a LH simulation with $N = 5000$ realizations, Figure 15 shows the natural frequency distribution for the first mode (bending) and the second mode (torsional) of this bridge with assigned uncertain parameters. It is readily observed that both distributions have a Gaussian shape. The blue line visualized the corresponding mean value.

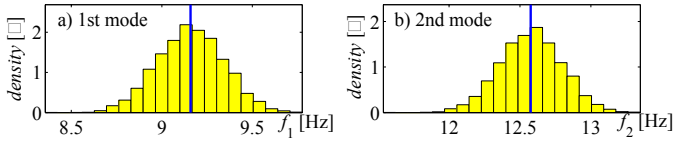

Figure 15. Distribution of the natural frequencies of the first and second mode.

When applying LS, for different design speeds v_0 important directions are evaluated according to Eq. (6). Therefor the partial derivative with respect to the kth random variable needed for $s(X_k)$ is evaluated as slope of the secant between its mean value μ_k and $\mu_k + 0.1\sigma_k$. In Figure 16 the entries e_k^{imp} of the importance vector $\mathbf{e}^{imp}$ are depicted for varying design speeds v_0. It is seen that the damping coefficient (X_{21}, deep blue) has a distinct influence on the maximum acceleration response. Moreover, also Young's modulus of the steel members (X_1), the ballast density (X_3) and height (X_4) are significant. From the remaining random variables, only the height of the web (X_{19}) of the right U-shaped girder and the ballast stiffness (X_5) have some influence at certain speeds.

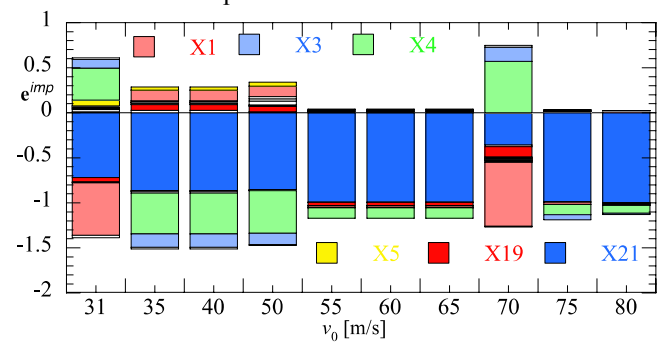

Figure 16. Important directions for line sampling as a function of discrete design speeds v_0.

6.3 *Reliability*

The response behavior of the bridge due to a change of its random parameters is basically the same as displayed in Figure 6. Variation of Young's modulus has the same impact on the response as illustrated by the red arrow in Figure 6. In this figure the blue arrow indicates the effect of uncertain bridge damping. However, variation of density, height and stiffness of the ballast and the remaining uncertain variables affect simultaneously response magnitude and resonance frequency. The important directions for the design speeds v_0 shown in Figure 16 are affected alike.

For design speeds $v_0 = 31.0$ and 70.0 m/s^2, respectively, five of the above mentioned random variables have a major influence on the important direction for finding the failure region. The positive values for e_3^{imp} and e_4^{imp} (X_3 and X_4) indicate that an increase of the mass leads to a rise of the peak acceleration response. Thus, changes in the resonance speeds are likely to move a new resonance peak within the considered speed range. The expected drop of the acceleration response for an increase of these parameters is observed for the other selected design speeds presented in Figure 16. For the design speeds v_0 = [55.0, 60.0, 65.0] m/s only the random damping value (X_{21}) leads to noteworthy changes of the peak acceleration.

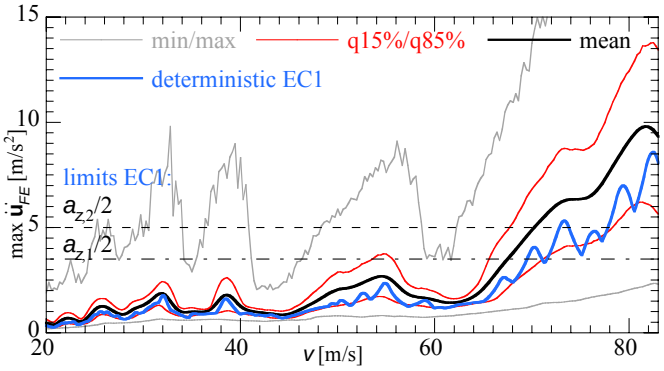

Figure 17. Spectrum of maximum acceleration induced by the HSLM-A train set for actual train speed v, elaborated bridge model.

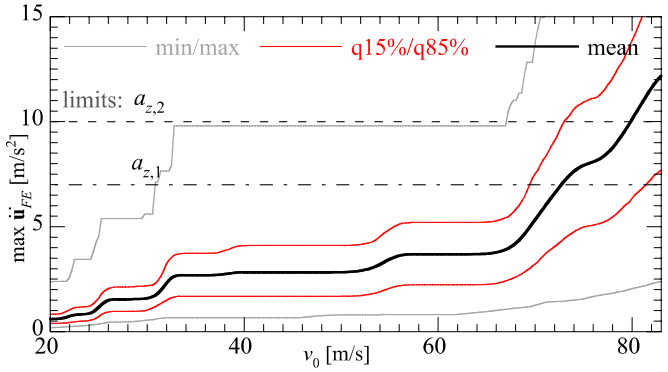

Figure 18. Spectrum of maximum acceleration induced by HSLM-A train set for design speed v_0, elaborated bridge model.

The spectral representation of the maximum acceleration response is computed with a LH sample using 5000 realizations. In Figure 17 and 18 the results of this simulation are represented by minimum, mean and maximum values, and 15% and 85% qauntile values, plotted against traveling and design speed v and v_0, respectively. Additionally, also the

peak acceleration of the deterministic model is shown. The deterministic assessment yields a limit of the maximum conceptual speed $v_E = 69.7 / 1.2 = 58.1$ m/s for the ballast stability limit $a_{z,1}$. In Figure 19 for the limits $a_{z,1}$ and $a_{z,2}$ an estimator for the failure probability is shown as a function of the design speed v_0. The results displayed with black and blue solid lines are evaluated with a LH sample of $N = 5000$ realizations. The dashed line represents the outcomes of the LS procedure with $N = 100$ realizations. The failure probability of $p_F = 10^{-4}$ required for $a_{z,1}$ is exceeded for all considered design speeds. With speeds higher than $v = 67.0$ m/s also the higher threshold $a_{z,2}$ yields not permitted values of $p_F > 10^{-6}$. In this example problem the variance is quite large. Moreover, the computed unit vectors $\boldsymbol{e}^{imp}$ point in the direction of locally increasing accelerations in the space of considered random parameters. The global directions may be different. Hence, larger samples ($N > 250$) are needed for the LS procedure to give accurate results also for the small values of p_F when the design speeds are small.

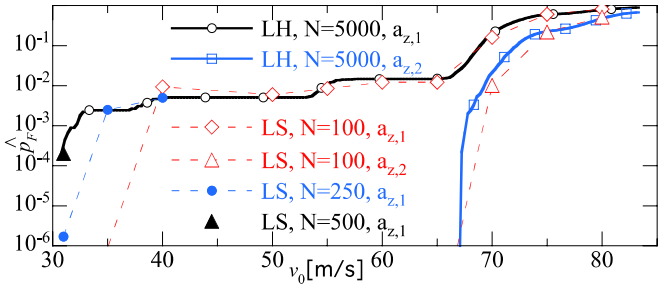

Figure 19. Estimates of the probability of failure for increasing design speed v_0, elaborated bridge model.

7 CONCLUSION

A probabilistic approach is used for estimating the reliability of railway bridges subjected to high-speed trains, with consideration of uncertain parameters. In this study the maximum acceleration response of the bridge is the governing response quantity. As simulation methods standard Monte Carlo simulations, Latin hypercube sampling and line sampling are used.

On a simple example bridge, additionally to uncertain viscous damping coefficients, the impact of a seasonal fluctuation of the environmental condition is modeled via a bilinear frequency-temperature relationship. Accordingly, stiffening of the structure due to frost shifts the resonance peaks to higher speeds and hence, the maximum acceleration response of the model are reduced.

For the more elaborated finite element model of a steel bridge, 21 uncertain parameters are considered. From these parameters, damping coefficient, ballast-height and -density and Young's modulus of the steel members have the largest influence on the dynamic bridge response.

The probability of failure for these two examples is governed via the likelihood of exceeding a certain threshold of the bridge deck acceleration. The simple example bridge shows good agreement with the outcome of an Eurocode based design.

The stochastic approach reveals that the elaborated example bridge does not satisfy the safety requirements when the train speed is larger than 30 m/s. In contrast, an Eurocode based design allows almost twice the travelling speed. This outcome depends however primarily on the chosen distribution of the damping coefficients, which are the governing quantity for the peak response in a state resonance.

For the simpler example problem line sampling is by far the most efficient method for the stochastic analysis. Since for the more elaborated model the variance of the bridge response is higher, larger samples are needed to predict reliably small failure probabilities.

REFERENCES

[1] Eurocode 0: EN1990: *Basis of structural design*, Brussels: CEN, 2002.

[2] Eurocode 1: EN1991-2: *Actions on structures - Part 2: traffic loads on bridges*, Brussels: CEN, 2003.

[3] UIC Leaflet 776-2, *Design requirements for rail-bridges based on interaction phenomena between train, track and bridge,* 2nd edition, 2009.

[4] P. Salcher and C. Adam, *Modelling strategies for bridges subjected to high-speed trains*, Proc. Vienna Congress on Recent Advances in Earthquake Engineering and Structural Dynamics (VEESD 2013), (C. Adam, R. Heuer, W. Lenhardt, C. Schranz, Eds), Austria, Vienna, 28.-30. Aug. 2013.

[5] Y.B. Yang, J.D. Yau and Y.S. Wu, *Vehicle-bridge interaction dynamics: with application to high-speed railways*, World Scientific Publishing, Singapore, 2004.

[6] L. Fryba, *Dynamics of railway bridges*. Thomas Telford, London, UK, 1996.

[7] I. Gonzales, M. Ülker-Kaustell and R. Karoumi, *Seasonal effects on the stiffness properties of a ballasted railway bridge*, Engineering Structures, 57, 63–72, 2013.

[8] B. Peeters and G. De Roeck, *One-year monitoring of the Z 24-Bridge: environmental effects versus damage events*, Earthquake Engineering & Structural Dynamics, 30, 149–171, 2001.

[9] P. Moser and B. Moaveni, *Environmental effects on the identified natural frequencies of the Dowling Hall Footbridge*, Mechanical Systems and Signal Processing, 25, 2336–2357, 2011.

[10] A. Tributsch, C. Adam, and G. Spielberger, *System identification of an old railway bridge subjected to varying environmental conditions*, Proc. 6th ECCOMAS Conference on Smart Structures and Materials (SMART2013), (E. Carrera, F. Miglioretti, M. Petrolo, Eds), Italy, Torino, 24-26 June, 2013.

[11] J. M. Rocha, A. A. Henriques and R. Calçada, *Safety assessment of a short span railway bridge for high-speed traffic using simulation techniques*, Engineering Structures, 40, 141–154, 2012.

[12] EUROPEAN STANDARD: EN 13450, *Aggregates for railway ballast*, Brussels: CEN, 2013.

[13] Joint Committee on Structural Safety (JCSS), *Probabilistic model code - 12th draft*, 2001. <http://www.jcss.ethz.ch/>

[14] UIC Report, *Design of New lines for Speed of 300 - 350 km/h - State of the Art Report*, 2001.

[15] A. Olsson, G. Sandberg and O. Dahlblom, *On Latin hypercube sampling for structural reliability analysis*, Structural Safety, 25, 47–68, 2003.

[16] C. Robert and G. Casella, *Monte Carlo statistical methods*, Springer-Verlag, New York, 2010.

[17] J.C. Helton and F.J. Davis, *Latin hypercube sampling and the propagation of uncertainty in analyses of complex systems*, Reliability Engineering & System Safety, 81, 23–69, 2003.

[18] P.S. Koutsourelakis, H.J. Pradlwarter and G.I. Schuëller, *Reliability of structures in high dimensions. Part I: algorithms and applications*, Probabilistic Engineering Mechanics, 19, 409–417, 2004.

[19] G.I. Schuëller, H.J. Pradlwarter and P.S. Koutsourelakis, *A critical appraisal of reliability estimation procedures for high dimensions*," Probabilistic Engineering Mechanics, 19, 463–474, 2004.

[20] H.J. Pradlwarter, *Relative importance of uncertain structural parameters. Part I: algorithm*, Computational Mechanics, 40, 627–635, 2006.